

Snow distribution, melt and surface water inputs to the soil in the mountain rain–snow transition zone



Patrick R. Kormos^{a,b,c,*}, Danny Marks^{d,1}, James P. McNamara^{a,2}, H.P. Marshall^{a,3}, Adam Winstral^{d,4}, Alejandro N. Flores^{a,5}

^aBoise State University, Department of Geosciences, 1910 University Dr., Boise, ID 83705, USA

^bU.S. Forest Service, Rocky Mountain Research Station, 322 E. Front St., Suite 401, Boise, ID 83702, USA

^cOak Ridge Institute for Science and Education, P.O. Box 117, Oak Ridge, TN 37831, USA

^dAgricultural Research Service, Northwest Watershed Research Center, 800 Park Blvd. Plaza IV, Suite 105, Boise, ID 83712, USA

ARTICLE INFO

Article history:

Received 28 September 2013

Received in revised form 30 April 2014

Accepted 28 June 2014

Available online 11 July 2014

This manuscript was handled by Konstantine P. Georgakakos, Editor-in-Chief, with the assistance of Daqing Yang, Associate Editor

Keywords:

Snowmelt
Surface water inputs
Soil water inputs
Snow model
Energy balance
Rain on snow

SUMMARY

The timing, magnitude, and spatial distribution of snow cover and the resulting surface water inputs (SWI) are simulated at a small catchment located in the rain–snow transition zone of southwest Idaho, USA. A physically based snow model is run on this 1.5 ha study catchment, which has an elevation range of 1600–1645 masl. The catchment is divided into relatively steep (mean slope angle of 21 degrees) northeast and southwest facing hill slopes by an ephemeral stream that drains to the southeast. SWI are fundamental controls on soil moisture, streamflow generation, groundwater recharge, and nutrient cycling. Although the timing of melt events is similar across the basin, southwest facing slopes receive smaller magnitude and more frequent SWI from mid winter snow melt, while the northeast facing slope receives greater SWI during the spring. Three spatial patterns are observed in the modeled SWI time series: (1) equal between slopes, (2) majority of SWI on southwest facing slopes, and (3) majority of SWI on northeast facing slopes. Although any of these three spatial patterns can occur during the snow season, four emergent SWI patterns emerge through the melt season: (1) near uniform, (2) controlled by topographic differences in energy fluxes, (3) transitional, and (4) controlled by snow distribution. Rain on snow (ROS) events produce similar SWI between the northeast and southwest facing slopes, with the difference being attributed primarily to snow distribution. Turbulent fluxes dominate the snowpack energetics in four of the five rain on snow events, and advective fluxes from precipitation are greater than 17% during the 2 rain on snow events in December and January. Net radiation fluxes dominate spring melt events. Variations in the method used to distribute precipitation may result in large differences in total precipitation to the basin.

© 2014 Elsevier B.V. All rights reserved.

1. Introduction

The hydrology of mountain basins is largely controlled by the distribution and timing of water delivery to the soil. Water

delivered to the soil, or surface water input (SWI), in a snow environment can originate by melt or rain draining from the snow cover or rain falling directly on the ground. The timing, magnitude, and spatial distribution of SWI to a catchment are fundamental controls on patterns of soil moisture (Seyfried et al., 2011, 2009; Williams et al., 2009), streamflow generation (Ali et al., 2012; Krajewski et al., 1991; Liu et al., 2013; Moore et al., 1991; Weill et al., 2013; McNamara et al., 2005), groundwater recharge (Aishlin and McNamara, 2011; Gee and Hillel, 1988; Scanlon et al., 2006), and nutrient cycling (Austin et al., 2004; Schmidt and Lipson, 2004). When rain falls on snow free ground, SWI is mainly dependent on the timing, magnitude, and distribution of precipitation, and secondarily dependent on vegetation interception processes. However, when precipitation falls as snow, or when the ground is snow covered regardless of precipitation phase, SWI

Abbreviations: SWI, surface water inputs; ROS, rain on snow; SCA, snow covered area; SWE, snow water equivalent; RMSE, root mean squared error.

* Corresponding author. Tel.: +1 (208) 921 1930.

E-mail addresses: patrickrkormos@fs.fed.us (P.R. Kormos), ars.danny@gmail.com (D. Marks), jmcmamar@boisestate.edu (J.P. McNamara), hpmarshall@boisestate.edu (H.P. Marshall), adam.winstral@ars.usda.gov (A. Winstral), lejoflores@boisestate.edu (A.N. Flores).

¹ +1 (208) 422 0721.

² +1 (208) 426 1354.

³ +1 (208) 426 1416.

⁴ +1 (208) 422 0739.

⁵ +1 (208) 426 2903.

is complicated by energy, climate, vegetation, and terrain factors. Snow cover temporarily stores water until it melts, so that SWI depends on the timing, magnitude, and distribution of precipitation, as well as the snow energy balance (Clark et al., 2011; Marks and Dozier, 1992; Marks and Winstral, 2001). Falling snow is susceptible to differential accumulation according to wind fields (Winstral and Marks, 2002; Winstral et al., 2009, 2013), and interception due to vegetation. Once on the ground, melt can be spatially heterogeneous due to vegetation and terrain factors that control solar and thermal radiation (Marks et al., 2002) and snowpack structure. A time lag may exist between snow melt and when it enters the ground as SWI due to the transmission properties of a layered snowpack (Colbeck, 1975), and/or the presence of basal ice (Woo et al., 1982). Melt water can move laterally within a sloping snowpack from the point of origin to the point where it enters the soil in a catchment (Eiriksson et al., 2013). Differential accumulation and melt by these factors can produce spatially discontinuous snow packs, which add new issues such as lateral energy transfer from bare soil to snow (Granger et al., 2002; Liston, 1995). Rain falling on discontinuous snow cover will further complicate the prediction of runoff from rain on snow (ROS) events. Several studies have documented the highly heterogeneous nature of snow water equivalent (SWE) on the ground (Anderton et al., 2004; Pomeroy et al., 2002), however few studies have taken the next step to investigate the more hydrologically relevant problem of heterogeneous SWI.

Slope aspect, henceforth referred to simply as aspect, impacts many of the processes that affect SWE and SWI in the mountainous western U.S. Wind can cause more snow to accumulate on lee versus windward slopes (Elder et al., 1991; Hiemstra et al., 2002; Luce et al., 1998; Winstral and Marks, 2002), aspect-driven differential insolation can cause melt heterogeneity (Elder et al., 1991; Marks and Dozier, 1992), and vegetation differences related to aspect can impose differential interception and snow trapping across a catchment (Gutierrez-Jurado and Vivoni, 2013; Ivanov et al., 2008; Molotch et al., 2009). Many studies have documented relationships between snow cover and terrain structure; solar-shaded slopes tend to store more SWE than solar-exposed slopes during melt, (Erxleben et al., 2002; Golding and Swanson, 1986; Jost et al., 2009, 2007; Williams et al., 2009), but few studies have addressed the influence of topography on snow distribution in shallow snow environments (see Winstral et al., 2009; Pomeroy et al., 2003; Pomeroy et al., 2013; Anderson et al., 2014) and these relationships may not hold from year to year (Dornes et al., 2008a,b; MacDonald et al., 2009; Pomeroy et al., 2004). The impact of aspect on SWI is less clear. For example, in a mountain catchment in Colorado, U.S., it was reported that snow accumulation was consistently higher on north facing versus south facing slopes (Hinckley et al., 2012). However, total seasonal SWI could be higher on south facing slopes because wind effects on the distribution of precipitation are dynamic.

SWI is further complicated in mid-elevation zones of the mountainous western U.S. near the margins of a continuous snowpack. This mid-elevation zone is commonly called the rain–snow transition zone. We define the rain–snow transition zone as the elevation band in temperate mountains where the dominant winter precipitation phase is variable, and changes from rain at lower elevations to snow at higher elevations. The elevation of this zone varies from sea level at high latitudes (Feiccabrinno et al., 2012) to over 2000 m at lower latitudes (Cayan et al., 2001). This zone typically occurs from 1500 m to 1800 m in the interior Pacific North-western U.S. and covers approximately 9200 km² (Nolin and Daly, 2006). The snow cover in this region is often thin and patchy, but may have significant depth resulting from a series of cold storms. The rain–snow transition zone is highly sensitive to small changes in temperature, and while changes may involve a small percentage

of the total SWI in a large catchment, they can potentially cause large changes in snow covered area (SCA). Due to the high albedo of snow, changes in SCA cause large changes in the energy balance of the ground surface.

Precipitation in the rain–snow transition zone can fall as rain or snow making the region highly susceptible to ROS events. These events often contribute to large floods (Kattelmann, 1996; Surfleet and Tullos, 2013) and major avalanche cycles (Conway and Raymond, 1993). While snow melt is generally enhanced during ROS events, the advective heat flux from the addition of water to the snowpack is not often the cause. Rather, the mechanism for increased snowmelt is generally recognized as an increase in turbulent energy fluxes associated with condensation during windy storm periods (Berris and Harr, 1987; Marks et al., 1998), although Mazurkiewicz et al. (2008) reported that an increase in net all-wave radiation could also be important at wind-protected sites.

Although the above mentioned complications have been overcome to varying degrees when simulating more continuous, seasonal snow packs (see Garen and Marks, 2005; Liston and Elder, 2006; Price and Dunne, 1976; Seyfried et al., 2009; Wigmosta et al., 1994), snow modeling is particularly difficult over an ephemeral snow cover in the rain–snow transition zone. In a mountain basin, the rain–snow transition zone typically occurs at the boundary between the snow- and rain-dominated regions. Snow simulation models, such as those cited above, have been optimized for the snow zone and, in general, are less effective over shallow ephemeral snow. Snow simulation studies within the rain–snow transition zone have had varying degrees of success. For example, a physically based snow model was applied to the same small catchment as the present study and reported an $r^2 = 0.22$ between measured and modeled SWE without accounting for wind redistribution of snow (Kelleners et al., 2010 & Kelleners et al., 2009). Small variations in forcing data and estimated precipitation distribution can result in large uncertainties over the shallow, ephemeral snow cover that “comes and goes” in the rain–snow transition zone. These uncertainties would have a negligible effect over a deeper and more substantial snow cover. Small variations in energy fluxes are capable of causing significant variations in snow temperature and/or melt because of the low thermal mass of a thin snow cover (Pomeroy et al., 2003; Williams et al., 2009). Ground heat is more important to the energetics of a thin snowpack. Shallow snow is further warmed by incoming solar radiation penetrating the snowpack and being absorbed and reemitted by low-lying vegetation and the ground surface (Knox et al., 2012), however the penetration depth of radiation is sensitive to snow grain size and density.

The goal of this study is to contribute to a greater understanding of the complex nature of the distribution of SWI to catchments in the rain–snow transition zone. This area is characterized by an ephemeral snowpack that is developed and ablated several times during the season. Understanding how SWI is generated and delivered to mountain basins in the rain–snow transition zones, and how these processes impact soil moisture, groundwater recharge, and streamflow is critical to managing water and ecosystems in western North America.

SWI is difficult to measure directly with conventional melt lysimeters because they alter ground–snow energy and mass exchanges, which are more important for shallow snow than for a deep snowpack. We therefore use a distributed, physically based snow accumulation and melt model in coordination with field observations to investigate SWI in a highly instrumented catchment in the rain–snow transition zone. Modeling snow cover in these shallow snow zones is important for understanding potential changes in the surface energy balance, caused by changes in SCA (Homan et al., 2011). Although simpler temperature index models have been applied over glaciers (Hock, 1999; Pellicciotti et al.,

2005), they are not appropriate over mountain basins, as shown by Walter et al. (2005) and more definitively by Kumar et al. (2013), where precipitation and surface energy fluxes are highly variable in space and time. For this investigation, we use a lidar-derived elevation dataset to distribute hourly time series data described in Kormos et al. (in preparation) to force and validate *iSnoval*, a distributed snow energy and mass balance model (Marks et al., 1999). *iSnoval* is a physically-based snow accumulation and melt model that has been successfully applied over many mountain basins in North America (e.g. Marks et al., 1999; Reba et al., 2014). Details about the *iSnoval* model, and the modeling approach are discussed in the Methods section of this paper.

We use the results from this modeling exercise to provide insight into (1) how rain and snow in this region control the timing and distribution of SWI, (2) the interaction between terrain structure, wind, precipitation distribution, and snow cover development, and (3) ephemeral snowpack energetics during ROS and spring melt events.

2. Study site

The Treeline experimental catchment is a 1.5 ha sub basin of the Dry Creek Experimental Watershed, established in 1999 to

investigate hydrologic processes in the semi-arid foothills 13 km north of Boise, Idaho (Fig. 1). The elevation of the Dry Creek Experimental Watershed ranges from 1030 to 2130 masl and consists of higher elevation forests that are snow-dominated and lower elevation grasslands that are rain-dominated. The Treeline catchment is a relatively steep catchment oriented approximately northwest-southeast, with a mean slope angle of 21 degrees and an elevation range from 1600 to 1645 masl, which conveniently situates it at both the vegetation and precipitation phase transition zones. The catchment boundary is delineated from a 1 m DEM originating from an airborne Lidar survey acquired in 2010 (Shallcross, 2012). Soils are thin (20–125 cm), sandy, and overlie biotite granodioritic bedrock (Williams et al., 2009). Vegetation on the northeast facing slope is typified by an abundance of *Artemisia tridentata* (Wyoming Big Sagebrush), *Ceanothus velutinus* (Buckbrush), *Prunus virginiana* (Chokecherry), as well as various forbs, and grasses (Patterson et al., 1985). Vegetation on the southwest facing slope is sparser and contains mostly grasses, forbs, and a few smaller shrubs. There are 8 conifer trees in the catchment that are assumed to have negligible influence on the catchment snow energy balance for the purpose of this study. Precipitation falls during the autumn, winter, and spring seasons and is largely absent from the summer months. The Treeline catchment received

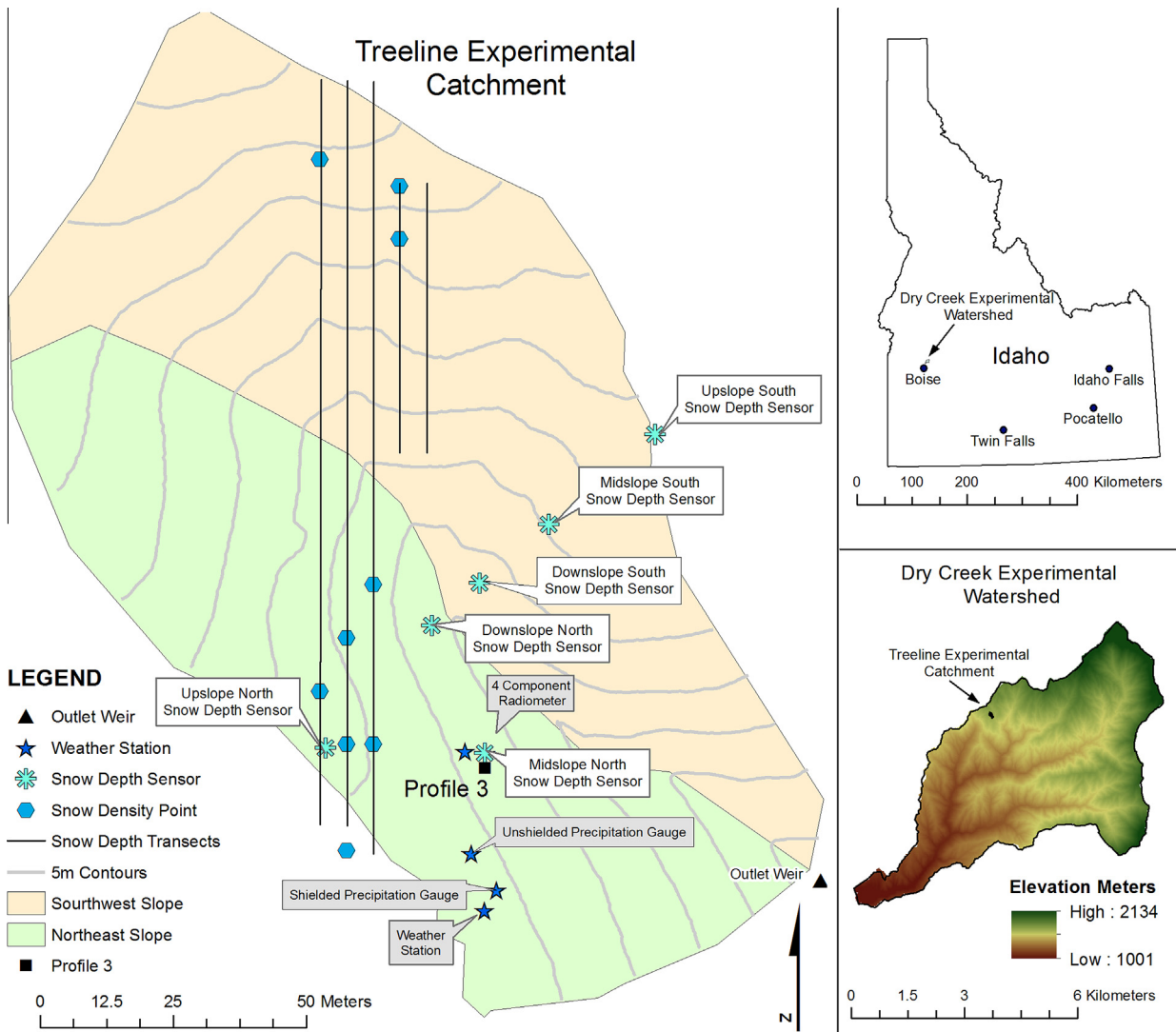


Fig. 1. Location map of the Treeline subcatchment of Dry Creek Experimental Watershed in Southwest Idaho showing instrument and measurement locations.

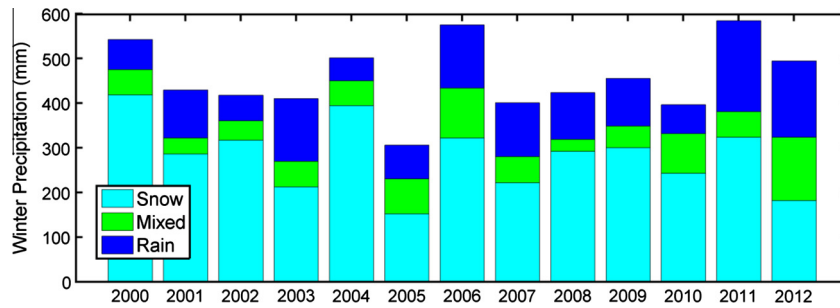


Fig. 2. Precipitation phase during winter months (October 1st–April 1st) showing the amount of rain, snow, and mixed events for the period of record.

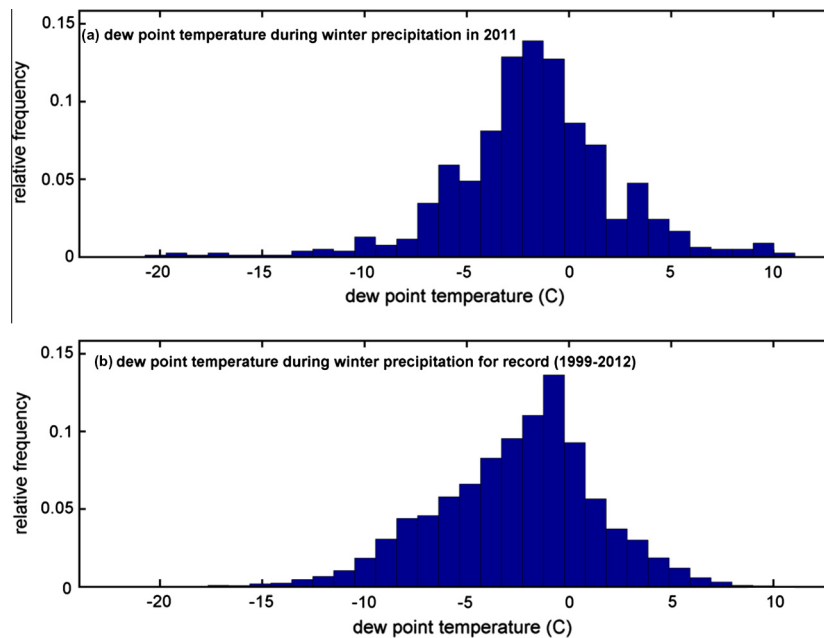


Fig. 3. Dew point temperature distribution during precipitation for winter months (October 1st–April 1st) showing (a) the WY2011 data compared to (b) the period of record (1999–2012).

approximately half of the winter precipitation (October 1st 2010–April 1st 2011) as rain or mixed events (Fig. 2). Most winter precipitation at Treeline falls when the dew point temperature is close to zero (Fig. 3). The mix of precipitation phase and the dew point temperature distribution for the period of record (Figs. 2 and 3b) at Treeline highlights the fact that it is situated within the rain–snow transition zone. Stream discharge from Treeline is intermittent, typically initiating in the early winter and ceasing in early summer (McNamara et al., 2005). Snow cover on the southwest facing slope tends to experience several full melt and accumulation cycles, while the northeast facing slope tends to retain a seasonal snowpack. Observed snow cover at Treeline differs with aspect. Given the small elevation range, elevation effects on the snow cover are undetectable.

The Treeline meteorological station and precipitation gauges are located on top of the northeast facing slope (Fig. 1). The model forcing and validation data from Treeline used in this study is described in detail in Kormos et al. (in preparation) and outlined briefly as follows. Air temperature, relative humidity, incoming solar radiation, average wind speed, and shielded and unshielded precipitation are recorded hourly at 2 m above the ground surface. Soil temperature is measured at a depth of 5 cm at Profile 3 on the northeast facing slope. Incoming and outgoing solar and thermal radiation are measured at a four-component radiometer (Hukseflux NR01, expected accuracy for daily sums: $\pm 10\%$) 2 m

above the ground surface on the northeast facing slope. Snow depth is recorded at six ultrasonic depth sensors that form a transect from the southwest ridge to the northeast ridge (Boe, 2013). Ten weekly snow surveys were conducted from January 21 to March 24, 2011. Between five and nine distributed snow density samples and 105–395 snow depths in 5 transects were collected in each survey, covering the range of snow conditions.

3. Methods

Surface water input (SWI) is water that enters the soil as rain, rain that passes through the snow, or melt water draining from the base of the snow. We simulated the distribution of SWI over the catchment using the *iSnobal* physically based distributed energy balance model to simulate the snow cover from October 1st, 2010 to October 1st, 2011 (WY2011). The *iSnobal* model (Marks et al., 1999) uses the catchment topography and distributed estimates of meteorological forcings to estimate the snow storage time series. *iSnobal* has been extensively applied and validated to investigate snow physics, processes, and the distributed melt patterns over complex terrain as well as ROS events at many locations within the mountains of western North America (Marks et al., 1998, 2001, 2002; Winstral and Marks, 2002; Winstral et al., 2009). The model simulates both the development and ablation of the snow cover, producing estimates of SWE, melt, liquid water

content, and SWI using input precipitation and available energy. The energy balance of the snowpack at each model pixel is expressed as:

$$\Delta Q = (R_{\text{net}} + H + L_v E + G + M)\Delta t, \quad (1)$$

where ΔQ is change in snowpack energy, and R_{net} , H , $L_v E$, G , and M are net radiative, sensible, latent, conductive, and advective (from precipitation) energy fluxes respectively (Marks and Dozier, 1992), and Δt is the time step. The model is forced by net solar, incoming thermal, air temperature, vapor pressure, wind speed, soil temperature, and precipitation. It represents the snow as a two-layer system, with a fixed-thickness surface layer, and a variable thickness lower layer representing the remainder of the snow cover. The model computes outgoing thermal radiation to get R_{net} , and solves for the rest of the energy balance. If ΔQ is negative, the snow will cool, increasing its “cold content” or the amount of energy required to bring the snow to 0 °C. If ΔQ is positive the snow will warm, reducing its cold content. Once the snow is at 0 °C, the cold content is zero, and any addition of energy will result in melt. If the addition of liquid water to the snow by either melt, or rain exceeds 1% (Davis et al., 1985), the excess is released to the soil as SWI. If the ground is not snow covered, the model passes precipitation that falls as rain to the soil as SWI.

All software utilities used for this research, including the *iSnoval* snow simulation model are available from *Software tools for hydro-climatic modeling and analysis: Image Processing Workbench, ARS-NWRC Version 2.1*, developed by the Northwest Watershed Research Center, USDA Agricultural Research Service, in Boise, ID (see <http://199.133.140.121/nwrc/ipw/intro.html>). The model was run at an hourly time step over a 2.5 m² DEM grid (2575 pixels). A high-resolution areal Lidar-derived topographic data set provided detailed topographic information, which made modeling at this fine spatial scale beneficial. The high spatial resolution explicitly resolves the ephemeral snow cover avoiding the need for sub-grid parameterization techniques such as depletion curves (Homan et al., 2011). Given that aspect is the main control on snow distribution at Treeline, this study focuses on the aspect-driven distribution of net radiation and wind-affected snow accumulation rates.

Net solar radiation is calculated from estimates of incoming solar radiation and albedo, and is provided to the model, along with incoming thermal radiation, as forcing parameters. Outgoing thermal radiation is calculated by the model from simulated active layer snow temperature. The model then calculates R_{net} from input net solar and incoming thermal, and computed outgoing thermal radiation. H and $L_v E$ are calculated from wind speed, air temperature, vapor pressure, and a uniformly distributed surface roughness parameter of 0.005 m. The roughness length was determined from previous simulations at similar locations (see Reba et al., 2014) and checked by inspection of point simulation results at the mid-slope snow depth sensor on the northeast facing slope. G is calculated from measured soil temperature and simulated snow temperature. Marks et al. (in press) showed definitively that, in the mountain environment, dew point temperature is equivalent to precipitation temperature. M is therefore based upon dew point temperature and precipitation mass. Horizontal advective heat fluxes are not taken into account in this study for simplicity, but may be an important flux when partial snow cover exists.

3.1. Net solar radiation

Clear sky incoming solar radiation was distributed over the DEM using the computer program *SToporad*, which calculates separate incoming clear-sky visible and near infrared solar radiation for each model pixel based on slope, aspect, and location of

the sun at each time step (Dozier, 1980; Dozier and Frew, 1981; Dubayah, 1994). The 2.5 m DEM extended a minimum of 80 m beyond the boundary of the catchment and was used to account for shading effects of adjacent topography. Calculated solar radiation values were corrected based on measured values from the weather station for each time step to account for cloud cover. Shading by vegetation canopy is considered negligible because of the low number of trees and the low-lying plant community that is quickly covered by snow accumulation. Spectral albedo is estimated from theoretical and empirical models for visible and near infrared wavelengths based on grain size and sun angle using methods presented by Marks and Dozier (1992). This method estimates the snow surface albedo resulting from each snow storm, and then accounts for the albedo decay over time from the last snowfall because of snow grain growth.

Calculated albedo was further degraded for litter and debris accumulation (Link and Marks, 1999) between maximum accumulation (March 30, 2011 at midnight) and snow disappearance (noon, April 12, 2011). A Lidar-derived raster of maximum vegetation height (Kormos et al., in preparation) was used to divide the Treeline catchment into 4 albedo decay zones: conifer tree, *Chokecherry*, windblown litter influence, and open. The conifer tree, and *Chokecherry* classes were determined for vegetation heights greater than 10 m, and between 2 and 10 m, respectively. The windblown litter zone was defined as the zone within 30 m from conifer trees. The open class contained all pixels less than 2 m height and more than 30 m from conifer trees. A time series of albedo decay factors were created for each class by linear interpolation:

$$\text{Albedo Decay Factor} = \left(\frac{(\text{max decay factor}) - 0}{t_{\text{meltout}} - t_{\text{peak}}} \right) \times t \quad (2)$$

where t is the time from peak accumulation, t_{meltout} and t_{peak} are the times of average snowpack melt out and peak accumulation respectively, and *max decay factor* is a parameter describing the maximum decrease in albedo expected from litter accumulation. Eq. (2) gradually increases the effect of litter accumulation on the snow surface from 0 at peak accumulation ($t = t_{\text{peak}} = 0$) to the maximum decay factor for that cover type at meltout ($t = t_{\text{meltout}}$). Maximum decay factors of -0.36 for conifers, -0.30 for *Chokecherry*, -0.27 for windblown litter, and -0.25 for open classes were used based on work from Winstral et al. (2013) and Reba et al. (2011a,b) in an area with similar vegetation. These decay factors were then added to the modeled visible and near infrared albedo values. Outgoing visible and near infrared solar radiation was obtained by multiplying the incoming solar radiation by the degraded albedo values.

3.2. Incoming thermal radiation

Clear sky incoming thermal radiation was distributed using TOPOTHERM, which accounted for elevation, air temperature, dew point temperature, and then corrected for adjacent terrain (Marks and Dozier, 1979). Calculated incoming thermal values were corrected based on measured values at the four component radiometer on the northeast facing slope (Kormos et al., in preparation) for each time step to account for cloud cover and atmospheric effects.

3.3. Temperature, wind speed, and humidity

Air temperature, ground temperature, and wind speed were uniformly distributed because the size of the catchment is small and contains minimal elevation changes. Vapor pressure and dew point temperature were calculated from measured air temperature and relative humidity, and were also uniformly distributed across

Table 1

Wind redistribution parameters and resulting RMSE between measured and modeled SWE. Average storm distributed precipitation for the whole catchment, northeast-, and southwest facing slopes are presented.

<i>dmax</i> (m)	<i>P1</i>	Inst. ht.(m)	Min. DAR	Sb ang. thresh. (degree)	RMSE (mm)	Precip. total (mm)	Precip. northeast facing slope (mm)	Precip. southwest facing slope (mm)
–	–	–	–	–	82.2	333	333	333
150	0.5	3	1.1	10	32.9	230	264	203
500	0.5	3	1.1	10	35.1	232	264	207
500	0.5	3	1.1	5	32.4	251	294	217
1000	0.5	3	1.1	5	32.6	255	301	219
500	0.6	3	1.1	5	37.1	270	305	241
500	0.55	3	1.1	5	34.2	260	300	229
500	0.5	3	1.2	5	36.5	263	313	223
150	0.5	2	1.1	5	36.7	260	301	228
500	0.5	2	1.1	5	36.6	259	297	228

the basin. Shallow soil temperatures (–5 cm) measured at Profile 3 were uniformly distributed across the catchment (Fig. 1).

3.4. Precipitation

Wind corrected precipitation (Hanson et al., 2004) was distributed following a modified version of the methods presented by Winstral et al. (2013). Liquid precipitation was distributed uniformly across the study area. Storms, which were defined as consecutive time steps with measured precipitation less than 3 h apart, were distributed if the storm-averaged dew point temperature was less than –0.5 °C and the storm total was more than 7 mm. The 7 mm threshold worked well at our study site, as it is common to receive many small storms. Larger thresholds excluded too many snow events, and smaller thresholds did not improve modeled results. Twenty storms met these criteria for WY2011. A unique accumulation ratio (AR), or fraction of the measured wind-corrected precipitation, for each pixel was calculated for each storm using the distributed maximum upwind slope (*Sx*) and slope break (*Sb*) parameters, both of which are functions of the topography and storm-averaged wind direction. *Sx* is calculated from a user-defined maximum search distance (*dmax*) and terrain obstruction height, referred to as *instrument height* by Winstral et al. (2009, 2013). *Sb* is the difference between local and outlying *Sx* calculations specified by a separation distance parameter. Drift zones are delineated as areas with *Sb* greater than a defined threshold. A separation distance of 60 m, based on previous modeling in a similar environment, was held constant during this exercise because it produced realistic precipitation distributions. The AR outside drift zones was obtained for each pixel using the empirical equation developed in Winstral et al. (2013) and modified using:

$$(1 - AR) \times P1 + AR, \quad (3)$$

where *P1* is a parameter that effectively reduced the difference between the original AR parameter and 1 (no modification to wind-corrected, measured precipitation) by a factor of *P1* (see Winstral et al., 2013). This method was used to make AR more applicable to areas with less wind scour than the area where the original equation was developed. The empirical equation presented in Winstral et al. (2013) to calculate AR for pixels within the drift zones (DAR) led to values of less than one for all storms. A minimum AR is imposed on areas within the drift zones. Without conducting a full sensitivity analysis, we objectively varied *dmax*, *Sb* angle threshold, *instrument height*, minimum DAR, and *P1* to achieve the lowest Root Mean Square Error (RMSE) between modeled and measured SWE from 14 locations in Treeline (Table 1). The 14 locations consisted of eight manually measured sites and six sites with ultrasonic depth sensors. The eight survey locations had at minimum 4 repeat SWE values. Snow depths measured at the six ultrasonic depth sensors on survey days are converted to SWE using a basin-averaged snow density from surveys. We use average snow

densities because slope-averaged differences in densities were not statistically significant.

4. Results

The *iSnobal* model performed well at the six ultrasonic snow depth sensors (Fig. 4). Accounting for wind redistribution decreased the RMSE between measured and modeled SWE at the 14 sites from 82.2 mm to approximately 35 mm (Table 1). However, the RMSE is relatively insensitive to the values that we have chosen to parameterize the redistribution model. Precipitation values in Table 1 are spatially averaged and include all precipitation from WY2011 snow storms. The model parameters used in this exercise resulted in precipitation range of 230–270 mm, with an average of 253. Distributed precipitation from storms was between 100 and 60 mm less than the 333 storm total from the uniform wind-corrected (measured) precipitation. The northeast facing slope received between 264 and 313 mm while the southwest facing slope received between 203 and 241 mm of storm totaled precipitation. The aspect differences in precipitation input have a significant impact on distributed hydrological processes and the catchment water balance.

For the purposes of this paper, we used the wind redistribution parameters that minimized discrepancies between measured and modeled SWE because that directly impacts the timing and magnitude of simulated SWI. The minimum RMSE of 32 mm between measured and modeled SWE at 14 locations in the catchment was achieved using the following parameters: *dmax* of 500 m, AR scaling parameter (*P1*) of 0.5, *instrument height* of 3 m, *minimum drift AR* of 1.1, and a *Sb* angle threshold of 5° (Table 1). The resulting precipitation input to the snow model provided a reasonable match to the observations. Errors between measured and modeled SWE and snow depths were within expected short length scale spatial variability. The midslope depth sensor on the northeast facing slope is adjacent to a ponderosa pine tree, which we assumed to have negligible influence on the basin SWE. However, decreased incoming solar radiation from shading may explain why the measured SWE was greater than modeled in January and February. The downslope depth sensor on the northeast facing slope is very close to the valley bottom and the head of the channel. Both the aspect and the slope are transitional here and small errors in the DEM have large impacts on the mass and energy balance due to uncertainty in true aspect. This site is also near to the bottom of the slope where the channel is typically filled with wind-blown snow during storms. This is a micro-scale process that may contribute to an increase in SWE at this location, but is not accounted for in the redistribution model. SWE measurements on the southwest facing slope are often near 50 mm after February when the model calculates no snow. The low thermal mass of this shallow snowpack is also very sensitive to small errors in energy balance

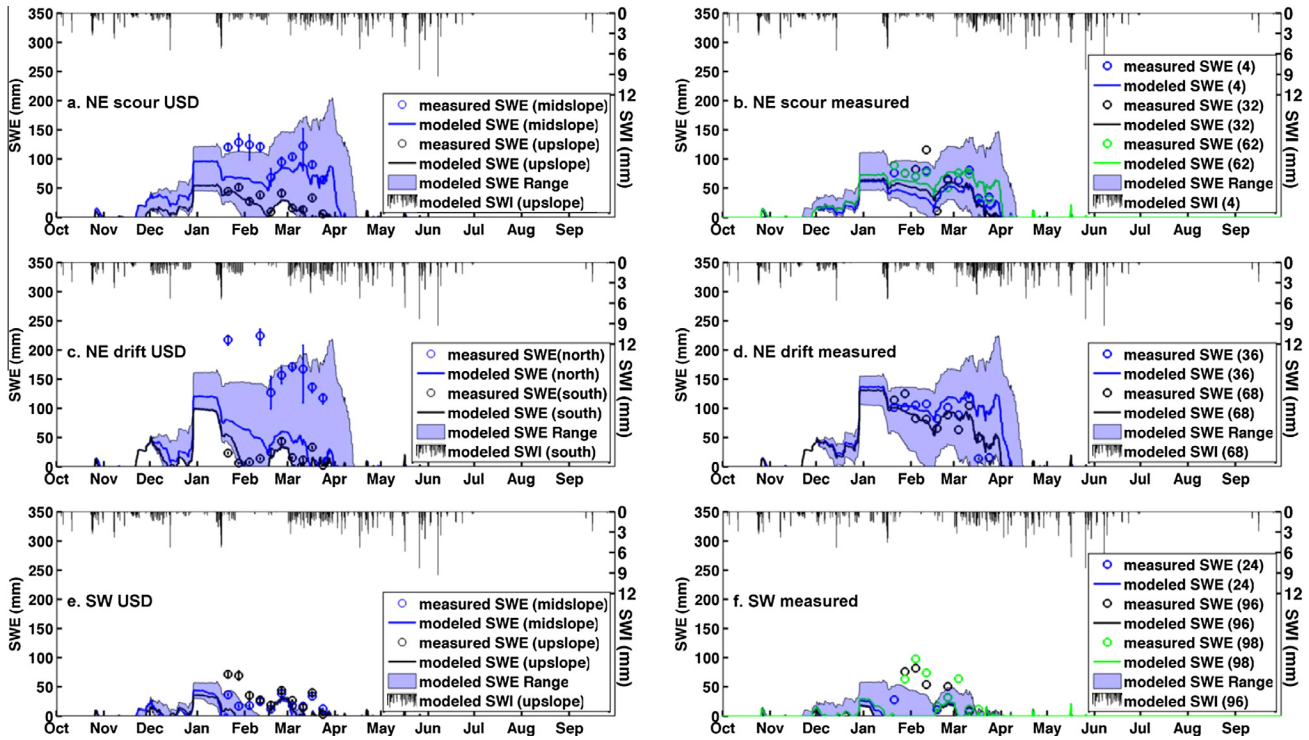


Fig. 4. Measured and modeled SWE at the 6 ultrasonic depth sensors (USD) (a, c, and e) and 8 measurement locations (MEAS) (b, d, and f). Error bars on depth sensor SWE values are the interquartile range of the snow depth at the time of the survey multiplied by all density measurements from that day. Solid lines indicate the modeled SWE at the pixel where the SWE measurement is located. The shaded regions depict the SWE range from the closest 25 model pixels within 5° of the Sb parameter (similar topographic characteristics) of the measurement location. Modeled SWI from specified measurement locations are represented by black bars on the reverse ordinate. Panels a and b are labeled scour because we expect less snow to be deposited here during redistribution. Panels c and d are labeled drift because we expect more snow to be deposited here during redistribution. Panels e and f are points from the southwest facing slope.

terms. These small errors in snow cover are expected to have minimal influence on the timing and magnitude of slope averaged SWI.

There is more snow stored on the northeast facing slope than the southwest facing slope (Fig. 4). Snow cover is also more continuous on the northeast facing slope, although the modeled SWE range reveals partial snow cover near all measurement locations for much of the winter. The average number of snow covered days on the northeast and southwest facing slopes is 143 and 87 days,

respectively (Fig. 5). Snow covered days are determined by the sum of the hourly time steps with SWE values greater than zero for all pixels on the slope, and converted to days. Although this difference was statistically significant at the 5% level, topographic variations on the northeast and southwest facing slopes that affect the radiation inputs and precipitation distribution lead to high variability in the snow covered day data.

The northeast facing slope had an average of 70 mm more total SWI than the southwest facing slope (Fig. 6) due to wind

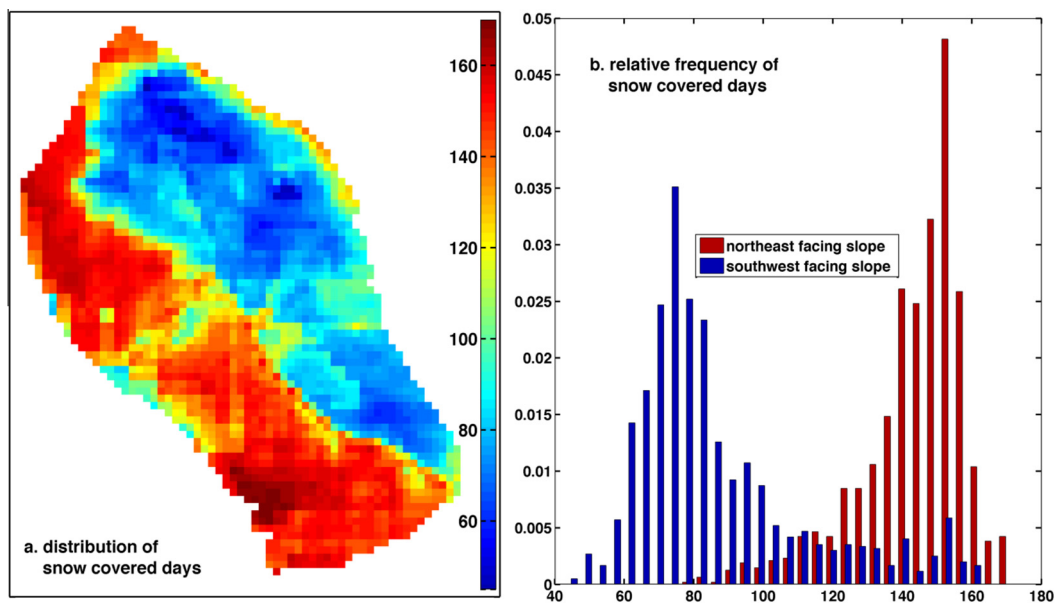


Fig. 5. (a) Snow covered days at the Treeline catchment for the WY2011. (b) The distribution of snow covered days by hill slope.

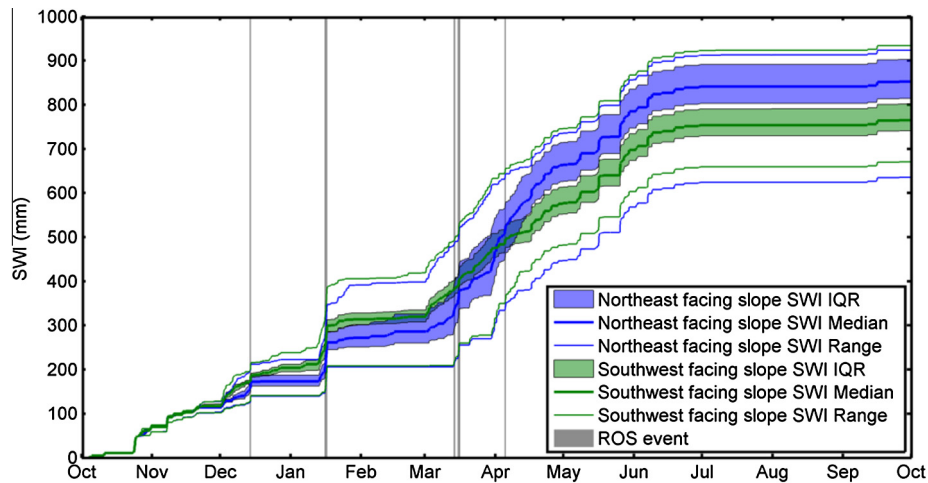


Fig. 6. Cumulative SWI from northeast- and southwest facing slopes at the Treeline catchment for WY2011. The timing of ROS events are shown as shaded grey regions.

redistribution depositing more snow on the northeast facing slope and scouring snow on the southwest facing slope. The wind redistribution procedure resulted in the northeast facing slope getting an average of 77 mm more precipitation than the southwest facing slope (Table 1). That difference is decreased by higher evaporation from the snowpack on the northeast facing slope (44 mm) compared to the southwest facing slope (37 mm). Though the southwest facing slopes have a greater propensity for evaporative losses because of wind exposure and higher insolation, the persistence of snowcover on the northeast facing slopes leads to greater net evaporation losses there. There is a high variability of SWI from both slopes as shown by the inter quartile range and full range of values in Fig. 6.

Time series of SWI at six locations across the catchment show that the timing of major melt events occurs simultaneously (Fig. 4). Snow melt events are smaller and more frequent on the southwest facing slope from December to mid January, resulting in a higher cumulative SWI during this period. Later melt events on the northeast facing slope begin February, and are larger than melt events on the southwest facing slope largely because there is more SWE. The northeast facing slope cumulative SWI exceeded that on the southwest facing slope beginning in early April.

Five ROS events occurred in WY2011 (Fig. 6 and Table 2). ROS events produced similar SWI between the northeast and southwest facing slopes, with the variations being attributed primarily to snow distribution. The magnitudes of energy fluxes depended on the time of year that the ROS event occurred. There was a switch from the dominant fluxes being turbulent in the winter, to a mix of turbulent and net all-wave radiation in the spring. Advective heat fluxes from precipitation were significant during the first two mid-winter ROS events. The northeast facing slope had a minimum of 3.6 times more SWE and 1.7 times more snow cover than the southwest facing slope at the onset of ROS events. A two-day spring melt event in which no measurable precipitation fell is included in Table 2 for comparison purposes. Radiation fluxes dominated this event.

SWI patterns at the Treeline catchment in WY2011 were controlled by the spatial distribution of snow and/or energy (Table 3, Fig. 7). Because simulated energy fluxes are unstable over thin, ephemeral snow, we limited the pixels used for the energy summary shown in Table 3 and Fig. 7 to those with a deeper snow cover (>100 mm SWE) for the entire two-week period indicated. Only bi-weekly periods from December 26, 2010 to May 1, 2011 had enough snow for this evaluation.

Three SWI patterns occurred in the Treeline catchment in WY2011: (1) equal between slopes, (2) greater on southwest facing slopes, and (3) greater on northeast facing slopes (Figs. 7, 8, and

Table 3). Although any of the three patterns can occur during a specific bi-weekly period, four emergent SWI periods progressed through the snow melt season: (1) near uniform SWI, (2) SWI patterns dominated by the distribution of energy, (3) transitional, and (4) SWI patterns dominated by the distribution of precipitation (Fig. 9). The transitional pattern (3) represents a switch in the dominant driving process responsible for the distribution of cumulative SWI from the distribution of the energy balance components to the distribution of precipitation. This is also the transition between the southwest facing slope receiving more cumulative SWI and the northeast facing slope receiving more cumulative SWI. The total SWI to Treeline for WY2011 was 812 mm. The SWI total for the snow season (November 20 to April 25) was 499 mm. The SWI during ROS events was 101 mm or approximately 12.5% of the total SWI and 20% of snow season SWI.

5. Discussion

5.1. Surface water input (SWI) distribution

SWI at the Treeline catchment is highly heterogeneous in time and space as a result of the complex interaction between the heterogeneous and ephemeral snow cover, energy balance, and precipitation distributions, all of which vary systematically with aspect. SWI in the rain–snow transition zone occurs throughout the winter season (Figs. 4 and 6). This is in contrast to higher elevation or colder catchments that have distinct accumulation and ablation periods, where the majority of SWI occurs during the spring melt. Although the timing of SWI from locations on northeast and southwest facing slopes appears to occur simultaneously, the magnitudes of SWI between slopes often vary. Contrasting SWI is likely to occur when there are differences in the amount of SCA on the two slopes. The differences in cumulative SWI between hill slopes highlight heterogeneous timing and magnitude of water availability for catchment processes beginning approximately December 1st (Fig. 6). This has implications for many catchment processes, including transpiration, streamflow source areas, and the distribution of deep percolation.

The three emergent spatial SWI patterns are a result of distributed energy inputs and precipitation distribution (Figs. 7, 8, and Table 3). Many time periods have near equal (<7.5 mm difference) SWI between slopes. These time periods are either characterized by having limited SCA on both slopes during precipitation events that include significant rain (panels 8a, 8b, 8n, & 8o), ROS events on ripe snow (panel 8f), or similar inputs of melt energy between slopes (ΔQ) (panels 8d, 8g, & 8h).

Table 2
Summary of the snow cover and mass and energy fluxes from the five ROS events that occurred at the Treeline catchment during WY2011. Energetics are slope averages for pixels with SWE greater than zero.

Rain on snow time period (mountain standard time) (start time + duration)	Precipitation (mm)		Total surface water input (mm)		Average SWE (mm)		SCA		Average net all-wave radiation flux (W/m ²)		Average turbulent flux (W/m ²)		Average ground heat flux (W/m ²)		Average advective heat flux (W/m ²)	
	Basin	Southwest facing slope	Southwest facing slope	Northeast facing slope	Northeast facing slope	Southwest facing slope	Northeast facing slope	Southwest facing slope	Northeast facing slope	Southwest facing slope	Northeast facing slope	Southwest facing slope	Northeast facing slope	Southwest facing slope	Northeast facing slope	Southwest facing slope
Dec. 14 6:00 (4 h.)	13	13	14	23	4	84	16	3.52	-7.04	9.63	1.63	1.66	5.10	5.10	5.10	5.10
Jan. 16 9:00 (16 h.)	34	41	48	101	28	100	58	13.23	13.15	39.97	1.86	2.37	11.95	11.95	11.95	11.95
Mar. 13 17:00 (13 h.)	8	8	12	106	17	83	11	-11.84	-24.25	45.72	1.23	1.19	0.74	0.74	0.74	0.74
Mar. 15 11:00 (14 h.)	23	18	29	95	16	80	10	24.01	20.08	25.94	1.52	1.45	4.94	4.12	4.12	4.12
Apr. 5 0:00 (11 h.)	12	12	13	68	12	59	8	18.91	3.81	6.82	1.54	1.45	1.19	1.19	1.19	1.19
Spring melt event Mar. 31 0:00 (48 h.)	0	5	34	109	17	79	9	34.39	19.33	0.67	7.89	10.08	-0.10	0.07	0.07	0.07
ROS SWI weighted energy fluxes	-	-	-	-	-	-	-	12.68	7.38	29.14	1.65	1.85	7.10	6.92	6.92	6.92

Time periods when southwest facing slopes produce more SWI (panels 8c, 8e, & 8i) are controlled by the distribution of energy flux terms. The two-week time period starting on November 28, 2010 resulted in 20 mm more SWI for the southwest facing slope (panel 8c), and was characterized by strong radiative cooling on the northeast facing slope that was not overcome by small positive turbulent fluxes. The southwest facing slope had positive net all-wave radiation and ground heat fluxes during this time. The two-week period beginning on December 26, 2010 had virtually no SWI to the northeast facing slope and an average of 10 mm SWI to the southwest facing slope. Melt on the southwest facing slope was caused by shallow snow energy dynamics, where the ground heat flux to pixels with a very thin snowpack is amplified. These fluxes are not represented in Table 3 or Fig. 7 because those pixels had SWE magnitudes less than the 100 mm cutoff. Spatially averaging G from all pixels with snow would result in a seemingly high magnitude of energy, even though the amount of snow involved (volumetrically) from those pixels would be very small. The biweekly period starting on February 20, 2011 resulted in 18 mm more SWI to the southwest facing slope. This time period had higher turbulent fluxes on the southwest facing slope (Table 3, Fig. 7), but was also dominated by shallow snow energy fluxes described above. Most pixels within the southwest facing shallow snowpack melted out completely, as SCA decreased from 88% to 42%.

Later in the season, when there are sufficient energy fluxes to produce consistent melt, more SWI is produced on northeast facing slope (panels 8j, 8k, 8l, & 8m). This is because the majority of the snow late in the season is on the northeast facing slope of the basin because of preferential retention of snow and precipitation redistribution during storms (Table 3 and Fig. 7).

Complex SWI patterns shown on panels 8f and 8j warrant further discussion. Panel 8f is the SWI from the biweekly time period starting January 9, 2011. This time period was dominated by the large January ROS event (Table 2). Wind redistribution of precipitation was not conducted for this time period because the event was mostly rain with warm dew point temperatures. The high magnitude of SWI during this biweekly period was the result of 77 mm of precipitation that fell during this time, 58 mm of which fell as rain. The SWI pattern on the southwest facing slope was controlled by the initial distribution of SWE, virtually all of which melted during the event. Patterns on the northeast facing slope were controlled by both the distribution of SWE and the distribution of energy balance terms.

In contrast, panel 8j shows SWI from the biweekly time period starting on March 6, 2011. The difference between these time periods is that three snow events, totaling over 60 mm of precipitation, were redistributed during this time. This distribution caused variability in SWI over the basin. The southwest facing slope had little snow at the beginning and end of this biweekly time period. All snow that fell on this slope melted by the end of this period. Although both slopes have approximately the same ΔQ by the end of this period, the northeast facing slope had more snow to melt, leading to a higher total SWI magnitude (Table 3 and Fig. 7).

Four characteristic SWI periods progressed with time in the rain-snow transition zone (Fig. 9). The first SWI pattern, shown in panels 9a & 9b, showed a near uniform pattern of SWI into the catchment, which resulted from: (1) early rain events (uniformly distributed), (2) early warm snow events that melted and did not develop into a snowpack, and (3) early cold snow events that developed into a snowpack, but did not begin to melt until later.

The second SWI pattern, shown in panels 9c–9i, was dominated by topographic differences in energy fluxes that occurred during the biweekly time periods starting on November 28, 2010 and February 20, 2011. These differences arose from topography related differences in the energy balance as described in the discussion of Fig. 8. Other time periods in this range had relatively uniform

Table 3
Biweekly snow cover information, mass fluxes, and energy fluxes to the snow pack. Energetics are slope averages for pixels with SWE greater than 100 mm.

Panel	Biweekly time period start	Precipitation (mm)		SWI (mm)		SWE (mm)		SWE (mm)		SCA (%)		Net radiation (W/m ²)		Turbulent flux (W/m ²)		Ground heat (W/m ²)		ΔQ (W/m ²)	
		northeast facing slope	southwest facing slope	northeast facing slope	southwest facing slope	northeast facing slope	southwest facing slope	northeast facing slope	southwest facing slope	northeast facing slope	southwest facing slope								
e	26-Dec-2010	69.6	0.1	95.7	10.5	97.5	44.5	100	97	-11.17	-12.07	2.36	3.46	7.23	6.84	-1.46	-1.60		
f	9-Jan-2011	77.5	95.7	102.2	99.3	102.2	33.7	100	77	-7.24	-11.73	6.81	8.89	7.00	6.65	7.35	4.59		
g	23-Jan-2011	2.2	11.4	88.9	8.6	88.9	18.3	96	23	-18.05	-18.15	8.42	9.12	8.81	9.14	0.19	0.12		
h	6-Feb-2011	25.3	11.5	80.6	5.8	80.6	17.5	91	35	-14.71	-15.31	8.20	9.61	8.88	8.58	2.34	2.86		
i	20-Feb-2011	30.1	15.1	104.8	33.1	104.8	34.3	100	88	-6.31	-7.68	1.42	2.86	5.98	5.80	1.09	1.03		
j	6-Mar-2011	79.4	85.1	106.3	70.8	106.3	19.2	93	42	0.90	-1.25	4.34	6.45	3.30	2.89	8.76	8.31		
k	20-Mar-2011	74.3	107.0	103.5	69.0	103.5	18.1	89	41	16.04	15.56	8.32	10.88	2.51	2.14	26.78	28.52		
l	3-Apr-2011	40.0	100.6	42.6	46.1	42.6	7.8	42	10	46.41	50.29	4.69	5.83	4.53	4.99	55.92	61.40		
m	17-Apr-2011	48.7	61.0	2.6	52.3	2.6	0.9	22	12	62.35	116.91	2.15	11.24	7.29	1.49	71.93	130.72		

SWI between slopes and merely sustained the pattern developed in Fig. 8c. These aspect related differences have been described in detail in earlier studies for the early ablation periods observed at sites with more continuous snow cover (see Pomeroy et al., 2003).

The third SWI pattern, depicted in panels 9j–9k, is transitional. This time period still showed aspect differences related to the energy balance, but also incorporated the distribution of snow cover resulting from differential melt and precipitation distribution.

The fourth SWI pattern, shown in panels 9l–9o, is controlled by the interaction between the distribution of snow over the catchment, higher sun angles, and warming conditions of spring. The combination of higher melt energy and SWE stored on northeast facing slopes led to the melt of all of the remaining snow on the northern aspects. All precipitation input to the basin (minus evaporation) entered the catchment soil system at this time.

ROS events produced similar SWI between the northeast and southwest facing slopes in the mountain rain–snow transition zone (Table 2). SWI values during ROS events were largely related to the amount of precipitation (Singh et al., 1997) and presence of snow cover. The snowpack was ripe preceding all five significant WY2011 ROS events, so there was no preferential retention of rain between slopes. The northeast facing slope often had a larger magnitude of SWI for time periods preceding and following the events largely because there was more snow to melt on northeast facing slopes (). The larger snow cover and magnitude of SWE on the northeast facing slope led to the 11 mm modeled difference in SWI between slopes for the March 15th ROS event.

Turbulent fluxes were the dominant source of energy input to the snowpack during the first four of the five WY2011 ROS events (Table 2). These events included the three largest ROS events that were responsible for over 10% of catchment SWI. Advective fluxes from precipitation contributed significant (at least 17%) energy fluxes during the first two mid winter ROS events. Higher net all-wave radiation values for the northeast facing slope in Table 2 were an artifact of deeper snow, greater SCA, and less wind exposure. Energy fluxes summarized in Table 2 were calculated only for snow-covered pixels.

Net radiation fluxes during the spring melt event accounted for about 80% of the melt energy (Table 2). This is in contrast to early ROS events where turbulent fluxes dominate the energy balance.

5.2. Implications of model forcing assumptions

Modeled results are inherently dependent on assumptions made by model users. Even physically based models such as *iSnobal* rely on assumptions made by developers concerning which processes require explicit representation and which can be simplified. *iSnobal* requires distributed forcing data at the spatial resolution chosen by the modeler. The most significant processes and forcing data, however, are not always apparent. For example, Anderson et al. (2014) demonstrate that the distribution of snow on the ground in Treeline is controlled not only by differential accumulation related to wind, but also by differential ablation related to solar loading. Site specific knowledge is essential to adequately force, calibrate, and validate physically based models. In this study, we show that the distributions of precipitation and radiation are essential in a rain–snow transition zone, even with low wind speeds, while reasonable results can be obtained without intensive distribution of other model drivers.

Simplifications were made during the distribution of model forcings for the WY2011 at the Treeline catchment. Air temperature and relative humidity were uniformly distributed across this small catchment with little impact on model results expected. Variation of these forcings over a small area and limited elevation range is negligible (Reba et al., 2011b). The ground temperature is expected to vary with topography when the snowpack is shallow

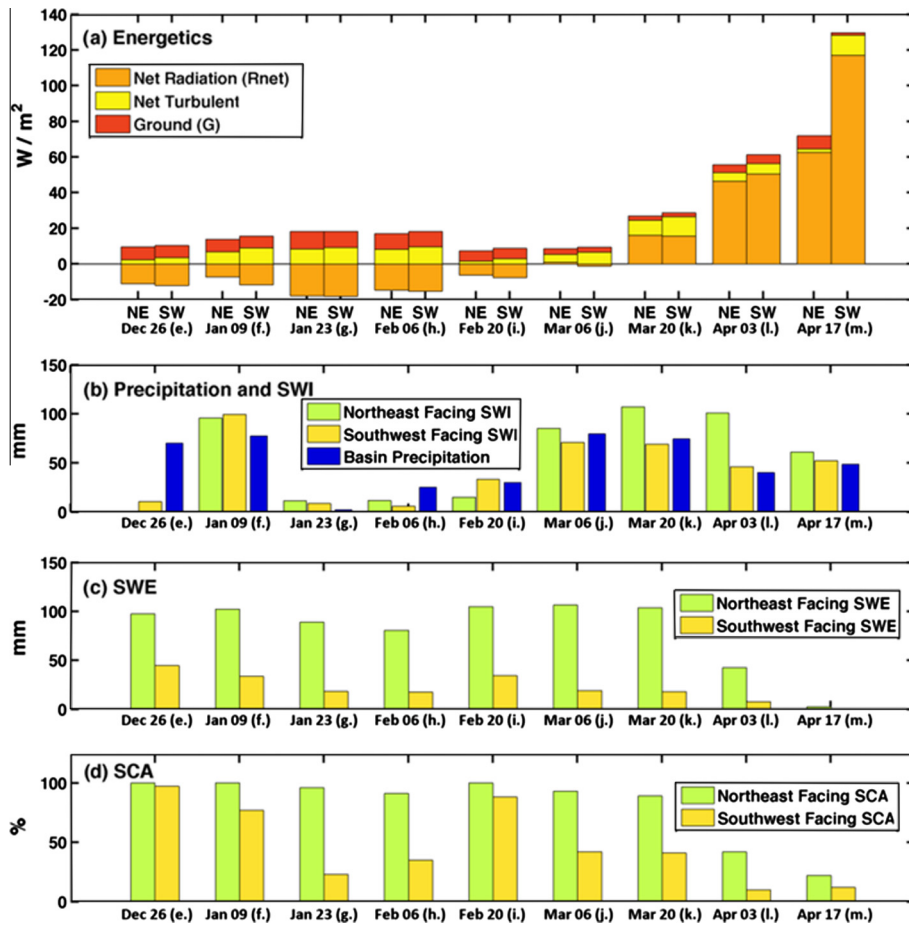


Fig. 7. Energetics (a), precipitation and SWI (b), SWE (c), and SCA (d) from biweekly time periods in Figs. 8 and 9.

due to the interaction of incoming solar radiation, aspect, and snow cover. Although the importance of the magnitude of G has been widely studied (Knox et al., 2012; Marks and Dozier, 1992; Marks et al., 1998; Mazurkiewicz et al., 2008; Pomeroy et al., 1998; Sensoy et al., 2006), there has been little research done on the spatial distribution of this term. Soil temperature, from which soil heat flux (G) is calculated, was uniformly distributed (Garen and Marks, 2005; Susong et al., 1999; Winstral and Marks, 2002), but is often linearly distributed with elevation on larger scales (Marks et al., 2001). It would not be unreasonable to set near surface soil temperature to $0\text{ }^{\circ}\text{C}$, as that is consistent with the snow temperature and the temperature of the melt water and SWI from the snow. However for this study we uniformly distribute the measured soil temperature from the single soil temperature measurement site within the catchment. We assume that the impact of soil temperature on G is small when there is a continuous, deep snow cover. However, the magnitude of G can be substantial when the snow cover is thin or ephemeral, based on this measured value. If we had more detailed information on soil temperature we would expect improved results. For example LaMontagne (2009) used fiber optic distributed temperature sensing (DTS) to show large differences in ground heat flux depending on the amount of snow cover at the Treeline catchment for WY2008. We also assume that the horizontal advective flux, or “local advection”, is negligible. This may be a significant flux when the snow is patchy. However, it is a function of wind speed and wind speeds are generally low in this study site. We acknowledge and accept these limitations to the modeling study, recognizing that the impact on SWE storage and SWI are minor.

Uniform wind speed distribution is an assumption that may have adverse effects on model results (Winstral and Marks, 2002;

Winstral et al., 2009). For example, turbulent fluxes can be quite different for exposed and sheltered sites as shown by Marks et al. (2002). This assumption disregards differences in turbulent fluxes associated with variable wind speeds across the catchment. Measured wind speeds from the WY2011 are generally low with a median value of 1.6 m/s and a 75th quantile of 2.8 m/s . These tower-measured wind speeds are at the lower limit of values used in empirical distribution models (Winstral et al., 2009), and would be further reduced at the surface due to topographic sheltering and vegetation that remains exposed above the snow. While the presence of a distributed wind component might have slightly improved model results, simulated turbulent energy fluxes would remain a very small component of the energy balance (Dadic et al., 2013).

Neglecting the influence of vegetation on incoming shortwave and thermal radiation could affect modeled SWE results. Due to the limited number of trees in the catchment, their effects on radiation terms are expected to have minimal influence on the overall basin SWE and SWI. Although it has been shown that grasses and shrubs in deeper snow packs are quickly covered by snow and compressed within a few centimeters of the ground surface (Menard et al., 2014), it is likely that the relatively shallow snow-pack allows for both the penetration of incoming solar radiation to warm this vegetation and contribute to melting, and for vegetation to protrude from the snow. *Chokecherry*, although taller than typical snow depths at the Treeline catchment, have small diameter stems with no leaves during the snow season and are observed to have minimal effects on snow accumulation and melt. Although we expect the influence of vegetation to be small, we recognize that it will have an influence on the snow dynamics. We expect

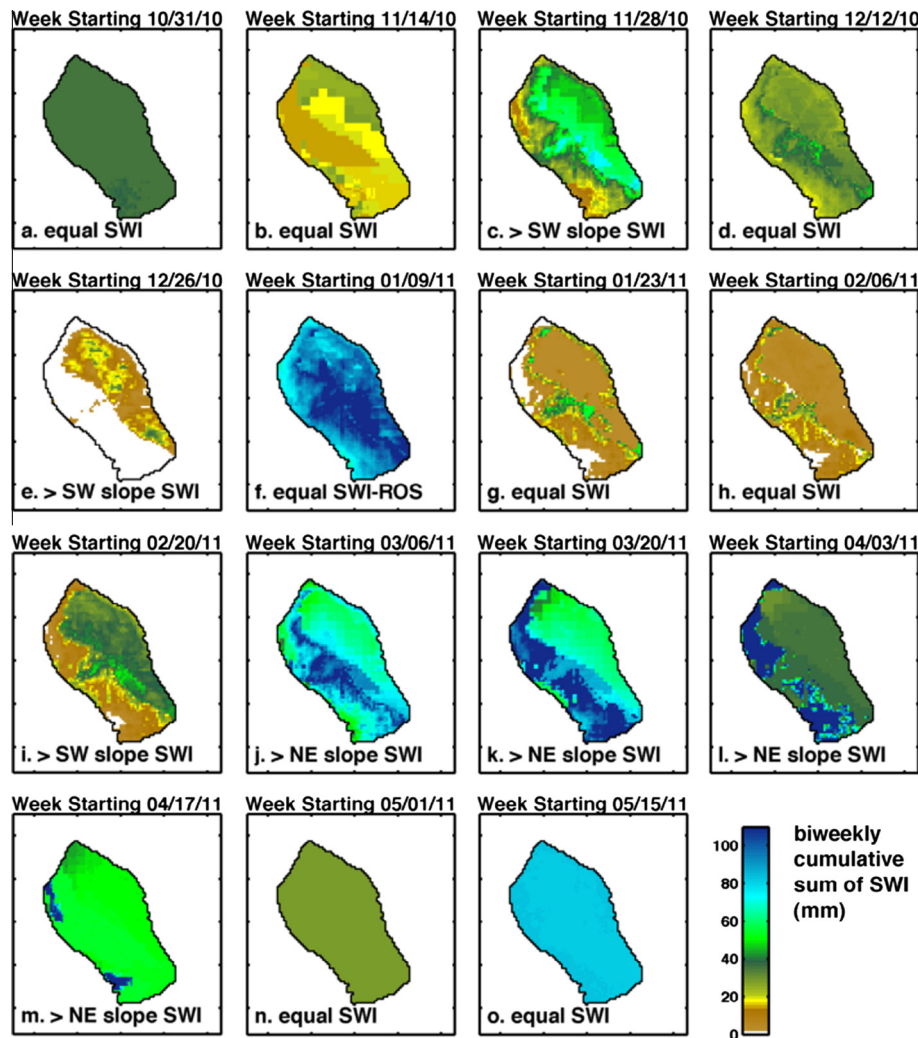


Fig. 8. Distributed biweekly incremental SWI from time periods beginning on October 31, 2010 through May 15, 2011.

that the model results would be improved by fully accounting for vegetation effects on the energy balance. For example, studies from arctic tundra indicate that short shrubs, such as the shrubs at the Treeline catchment, are exposed rapidly once snow depths decline below shrub height (Pomeroy et al., 2006). Once shrubs are exposed, the snow melt rate increases as radiative and turbulent transfer increase. Melt rates have been shown to increase by up to 7% for wind speeds of 2 m s^{-1} depending on snow cover and snow patch size (Liston, 1995). Another facet of vegetation influences on snow dynamics that may be improved in the model would be shrub bending effects on albedo, which has been shown to improve snow model results (Menard et al., 2014).

The simulation methods used in this study rely on the efficacy of the *iSnobal* model physics, the assumption that spatially distributed model forcings are accurate, and that the precipitation distribution can be approximated from measured wind, precipitation, and temperature. The parameters of the empirical snow redistribution procedure presented were varied to obtain a reasonable fit between measured and modeled SWE. We recognize that this method may affect model results beyond the influence of wind. For example, energy balance terms may be systematically low on south facing slopes, which would result in more modeled snow compared to measurements. This could result from the uniform distribution of ground temperatures from the northeast facing slope or neglecting vegetation. The optimization of the wind redistribution model would essentially compensate for an

underestimation of melt by scouring more snow. However, parameters used vary only slightly from those suggested in the literature (Winstral and Marks, 2002; Winstral et al., 2009, 2013) (Table 1). Choosing to distribute precipitation from wind during snow storms, rather than uniformly distributing wind corrected precipitation over the entire season, decreased the RMSE by approximately 50 mm of SWE.

The wind redistribution parameter set has implications on both the magnitude and distribution of precipitation during storms, which has cascading consequences for SWI differences between slopes and catchment mass balance studies (Fig. 6 and Table 1). Distributing precipitation using wind speed and direction during snow storms, rather than uniformly distributing wind-corrected precipitation from the gauge, decreased the precipitation inputs by as much as 100 mm. A difference of 40 mm of basin average precipitation is possible depending on the wind distribution parameters used. The small range from 32 to 37 mm in the RMSE associated with parameter set choice substantiates the robustness of the wind redistribution model (Table 1). We recognize that our measurement dataset may not be sufficient to say what parameter set produces a precipitation data set that is closest to the actual distribution. Although this error is a significant percentage of the shallow snowpack in the rain-snow transition zone, it is a significant accomplishment when compared to the requirement of 30 mm SWE accuracy for shallow snow in the current mission concepts for both the European Space Agency Cold Regions

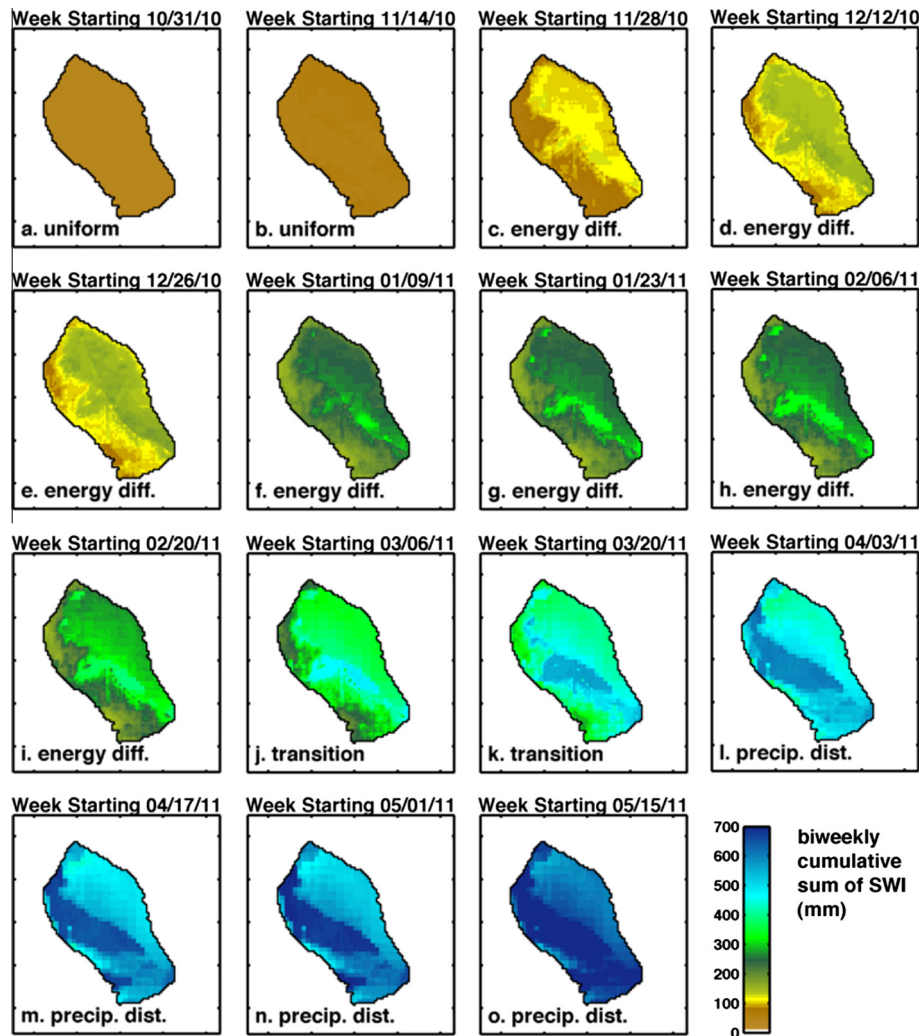


Fig. 9. Distributed biweekly cumulative SWI from time periods beginning on October 31, 2010 through May 15, 2011.

High-resolution Hydrologic Observatory (CoReH2O) and NASA Snow and Cold Lands Processes (SCLP) future proposed satellites (Rott et al., 2009, 2010).

The wind redistribution of precipitation during snow events led to a maximum of 90 mm difference in slope-averaged precipitation for the northeast and southwest facing slopes. Quantifying the spatial precipitation inputs to a catchment is critical to distributed catchment modeling. This is highlighted in the 70 mm difference in cumulative SWI between slopes by the end of WY2011, which is primarily a result of the precipitation distribution (Fig. 6).

6. Conclusions

Snow and resulting SWI distributions from the rain–snow transition zone are dynamic and largely aspect dependent. Northern aspects stored more snow and have a more continuous snow cover than southern aspects. Mid winter SWI at the Treeline catchment occurred more frequently on the southwest facing slopes, while SWI on northeast facing slopes increased during spring. Four characteristic SWI periods occurred at the Treeline catchment: (1) near uniform, (2) controlled by topographic differences in energy fluxes, (3) transitional, and (4) controlled by snow distribution. ROS events produced similar magnitudes of SWI between northeast and southwest facing slopes in the Treeline catchment. ROS events contributed 12.5% of the total and 20% of the snow season SWI at

the Treeline catchment in WY2011. Turbulent fluxes dominated the energy balance during all but one of the ROS events. Net all-wave radiation fluxes dominated the energy balance during spring melt. Advective fluxes from precipitation were greater than 17% of the energy balance during the first two ROS events. Distributing precipitation resulted in large decreases in modeled SWE errors. The different combinations of precipitation distribution parameters that we explored at the Treeline catchment resulted in a change of as much as 100 mm of total precipitation and a 90 mm difference between northeast and southwest facing slopes for WY2011. This study also showed that it is possible to simulate the distribution of snow, melt energetics, and SWI over the dynamic and ephemeral snow cover in the rain–snow transition zone.

7. Data availability

Model forcing and validation data used in this paper are described in Kormos et al. (in preparation) and are freely available at <http://doi.pangaea.de/10.1594/PANGAEA.819837>. Included are readme files in each directory listing the data contents, a detailed description of data, and contact information for additional details. Distributed model forcings and results are available from the authors upon request.

Acknowledgements

The data and analysis presented in this paper were funded in part by NASA EPSCoR and INRA, NSF-CBET (0854553, 08522), USDA-ARS CRIS Snow and Hydrologic Processes in the Intermountain West (5362-13610-008-00D), USDA-NRCS Water and Climate Center-Portland, Oregon (5362-13610-008-03R), NSF-EPS (0919514), and NOAA (NA08NWS4620047). The USDA Northwest Watershed Research Center and Boise State University Department of Geosciences, Student Research Initiative, and Graduate College provided funding, travel and general support for the project. We want to specifically thank Mark Seyfried, Erik Boe, Pam Aishlin, Justin Huntington, and Molly Gribb for generous assistance with data collection and preparation of the paper. Any reference to specific equipment types or manufacturers is for information purposes and does not represent a product endorsement or recommendation. Boise State University and the USDA ARS are equal opportunity employers.

References

- Aishlin, P., McNamara, J.P., 2011. Bedrock infiltration and mountain block recharge accounting using chloride mass balance. *Hydrol. Process.* 25 (12), 1934–1948. <http://dx.doi.org/10.1002/hyp.7950>.
- Ali, G., Tetzlaff, D., Soulsby, C., McDonnell, J., 2012. Topographic, pedologic and climatic interactions influencing streamflow generation at multiple catchment scales. *Hydrol. Process.* 26 (25), 3858–3874. <http://dx.doi.org/10.1002/hyp.8416>.
- Anderson, B.T., McNamara, J.P., Marshall, H.P., Flores, A.N., 2014. Insights into the physical processes controlling correlations between snow distribution and terrain properties. *Water Resour. Res.* 50. <http://dx.doi.org/10.1002/2013WR013714>.
- Anderton, S.P., White, S.M., Alvera, B., 2004. Evaluation of spatial variability in snow water equivalent for a high mountain catchment. *Hydrol. Process.* 18 (3), 435–453. <http://dx.doi.org/10.1002/hyp.1319>.
- Austin, A. et al., 2004. Water pulses and biogeochemical cycles in arid and semiarid ecosystems. *Oecologia* 141 (2), 221–235. <http://dx.doi.org/10.1007/s00442-004-1519-1>.
- Berris, S.N., Harr, R.D., 1987. Comparative snow accumulation and melt during rainfall in forested and clear-cut plots in the western cascades of Oregon. *Water Resour. Res.* 23 (1), 135–142. <http://dx.doi.org/10.1029/WR023i001p00135>.
- Boe, E., 2013. Assessing Local Snow Variability Using a Network of Ultrasonic Snow Depth Sensors. Boise State University, Boise, ID, 72 pp.
- Cayan, D.R., Kammerdiener, S.A., Dettinger, M.D., Caprio, J.M., Peterson, D.H., 2001. Changes in the onset of spring in the western United States. *Bull. Am. Meteorol. Soc.* 82 (3), 399–415. [http://dx.doi.org/10.1175/1520-0477\(2001\)082<0399:citoos>2.3.co;2](http://dx.doi.org/10.1175/1520-0477(2001)082<0399:citoos>2.3.co;2).
- Clark, M. et al., 2011. Representing spatial variability of snow water equivalent in hydrologic and land-surface models: a review. *Water Resour. Res.* 47, W0753910.1029/2011wr010745.
- Colbeck, S.C., 1975. Theory for water-flow through a layered snowpack. *Water Resour. Res.* 11 (2), 261–266. <http://dx.doi.org/10.1029/WR011i002p00261>.
- Conway, H., Raymond, C.F., 1993. Snow stability during rain. *J. Glaciol.* 39 (133), 635–642. <Go to ISI>://WOS:A1993NA69200022.
- Dadic, R. et al., 2013. Sensitivity of turbulent fluxes to wind speed over snow surfaces in different climatic settings. *Adv. Water Resour.* 55, 178–189. <http://dx.doi.org/10.1016/j.advwatres.2012.06.010>.
- Davis, R.E., Dozier, J., LaChapelle, E.R., Perla, R., 1985. Field and laboratory measurements of snow liquid water by dilution. *Water Resour. Res.* 21 (9), 1415–1420. <http://dx.doi.org/10.1029/WR021i009p01415>.
- Dornes, P.F., Pomeroy, J.W., Pietroniro, A., Verseghy, D.L., 2008a. Effects of spatial aggregation of initial conditions and forcing data on modeling snowmelt using a land surface scheme. *J. Hydrometeorol.* 9, 789–803. <http://dx.doi.org/10.1175/2007JHM958.1>.
- Dornes, P.F., Pomeroy, J.W., Pietroniro, A., Carey, S.K., Quinton, W.L., 2008b. Influence of landscape aggregation in modelling snow-cover ablation and snowmelt runoff in a sub-arctic mountainous environment. *Hydrol. Sci. J.* 53 (4), 725–740. <http://dx.doi.org/10.1623/hysj.53.4.725>.
- Dozier, J., 1980. A clear-sky spectral solar-radiation model for snow-covered mountainous terrain. *Water Resour. Res.* 16 (4), 709–718. <http://dx.doi.org/10.1029/WR016i004p00709>.
- Dozier, J., Frew, J., 1981. Atmospheric corrections to satellite radiometric data over rugged terrain. *Remote Sens. Environ.* 11 (3), 191–205. [http://dx.doi.org/10.1016/0034-4257\(81\)90019-5](http://dx.doi.org/10.1016/0034-4257(81)90019-5).
- Dubayah, R.C., 1994. Modeling a solar-radiation topoclimatology for the Rio-Grande River Basin. *J. Vegetat. Sci.* 5 (5), 627–640. <<http://www.jstor.org/stable/3235879>>.
- Eiriksson, D. et al., 2013. An evaluation of the hydrologic relevance of lateral flow in snow at hillslope and catchment scales. *Hydrol. Process.* 27 (5), 640–654. <http://dx.doi.org/10.1002/hyp.9666>.
- Elder, K., Dozier, J., Michaelsen, J., 1991. Snow accumulation and distribution in an alpine watershed. *Water Resour. Res.* 27 (7), 1541–1552. <http://dx.doi.org/10.1029/91wr00506>.
- Erleben, J., Elder, K., Davis, R., 2002. Comparison of spatial interpolation methods for estimating snow distribution in the Colorado Rocky Mountains. *Hydrol. Process.* 16 (18), 3627–3649. <http://dx.doi.org/10.1002/hyp.1239>.
- Feiccabrinio, J., Lundberg, A., Gustafsson, D., 2012. Improving surface-based precipitation phase determination through air mass boundary identification. *Hydrol. Res.* 43 (3), 179–191. <http://dx.doi.org/10.2166/nh.2012.060>.
- Garen, D.C., Marks, D., 2005. Spatially distributed energy balance snowmelt modelling in a mountainous river basin: estimation of meteorological inputs and verification of model results. *J. Hydrol.* 315 (1–4), 126–153. <http://dx.doi.org/10.1016/j.jhydrol.2005.03.026>.
- Gee, G.W., Hillel, D., 1988. Groundwater recharge in arid regions – review and critique of estimation methods. *Hydrol. Process.* 2 (3), 255–266. <http://dx.doi.org/10.1002/hyp.3360020306>.
- Golding, D.L., Swanson, R.H., 1986. Snow distribution patterns in clearings and adjacent forest. *Water Resour. Res.* 22 (13), 1931–1940.
- Granger, R., Pomeroy, J., Parviainen, J., 2002. Boundary-layer integration approach to advection of sensible heat to a patchy snow cover. *Hydrol. Process.* 16 (18), 3559–3569. <http://dx.doi.org/10.1002/hyp.1227>.
- Gutierrez-Jurado, H.A., Vivoni, E.R., 2013. Ecogeomorphic expressions of an aspect-controlled semiarid basin: II. Topographic and vegetation controls on solar irradiance. *Ecology* 6 (1), 24–37, doi: 10.1002/eco.1263. doi: 10.1029/WR022i013p01931.
- Hanson, C.L., Pierson, F.B., Johnson, G.L., 2004. Dual-gauge system for measuring precipitation: historical development and use. *J. Hydrol. Eng.* 9 (5), 350–359. [http://dx.doi.org/10.1061/\(ASCE\)1084-0699\(2004\)9:5\(350](http://dx.doi.org/10.1061/(ASCE)1084-0699(2004)9:5(350).
- Hiemstra, C.A., Liston, G.E., Reiners, W.A., 2002. Snow redistribution by wind and interactions with vegetation at upper treeline in the Medicine Bow Mountains, Wyoming, USA. *Arctic Antarctic and Alpine Research* 34 (3), 262–273. <http://dx.doi.org/10.2307/1552483>.
- Hinckley, E.-L.S., Ebel, B.A., Barnes, R., Anderson, R.S., Williams, M.W., Anderson, S.P., 2012. Aspect control of water movement on hillslopes near the rain–snow transition of the Colorado Front Range. *Hydrol. Process.* <http://dx.doi.org/10.1002/hyp.9549>.
- Hock, R., 1999. A distributed temperature-index ice- and snowmelt model including potential direct solar radiation. *J. Glaciol.* 45(149), 101–111 <Go to ISI>://WOS:00080138700012.
- Homan, J., Luce, C., McNamara, J., Glenn, N., 2011. Improvement of distributed snowmelt energy balance modeling with MODIS-based NDSI-derived fractional snow-covered area data. *Hydrol. Process.* 25 (4), 650–660. <http://dx.doi.org/10.1002/hyp.7857>.
- Ivanov, V.Y., Bras, R.L., Vivoni, E.R., 2008. Vegetation-hydrology dynamics in complex terrain of semiarid areas: 1. A mechanistic approach to modeling dynamic feedbacks. *Water Resour. Res.* 44 (3), 34, W0342910.1029/2006wr005588.
- Jost, G., Weiler, M., Gluns, D.R., Alila, Y., 2007. The influence of forest and topography on snow accumulation and melt at the watershed-scale. *J. Hydrol.* 347 (1–2), 101–115. <http://dx.doi.org/10.1016/j.jhydrot.2007.09.006>.
- Jost, G., Moore, R.D., Weiler, M., Gluns, D.R., Alila, Y., 2009. Use of distributed snow measurements to test and improve a snowmelt model for predicting the effect of forest clear-cutting. *J. Hydrol.* 376 (1–2), 94–106. <http://dx.doi.org/10.1016/j.jhydrol.2009.07.017>.
- Kattelmann, 1996. Flooding from rain-on-snow events in the Sierra Nevada. In: Leavesley, G.H.L., Harry F. Nobilis, Franz Parker, Randolph S. Schneider, Verne R. van de Ven, Frans H.M. (Eds.), *Destructive Water: Water-Caused Natural Disasters—Their Abatement and Control*. Red Books. IAHS, Anaheim, California, pp. 59–65.
- Kelleners, T.J., Chandler, D.G., McNamara, J.P., Gribb, M.M., Seyfried, M.S., 2009. Modeling the water and energy balance of vegetated areas with snow accumulation all rights reserved. No part of this periodical may be reproduced or transmitted in any form or by any means, electronic or mechanical, including photocopying, recording, or any information storage and retrieval system, without permission in writing from the publisher. *Vadose Zone J.* 8 (4), 1013–1030. <http://dx.doi.org/10.2136/vzj2008.0183>.
- Kelleners, T.J., Chandler, D.G., McNamara, J.P., Gribb, M.M., Seyfried, M.S., 2010. Modeling Runoff Generation in a Small Snow-Dominated Mountainous Catchment All rights reserved. No part of this periodical may be reproduced or transmitted in any form or by any means, electronic or mechanical, including photocopying, recording, or any information storage and retrieval system, without permission in writing from the publisher. *gsvadzone*, 9(3), 517–527 doi: 10.2136/vzj2009.0033.
- Knox, S.H., Carey, S.K., Humphreys, E.R., 2012. Snow surface energy exchanges and snowmelt in a shrub-covered bog in eastern Ontario, Canada. *Hydrol. Process.* 26 (12), 1877–1891. <http://dx.doi.org/10.1002/hyp.9289>.
- Kormos, P.R., Marks, D., Williams, C.J., Marshall, H.P., Aishlin, P., Chandler, D.G., McNamara, J.P., 2013. Soil, snow, weather and sub-surface storage data from a mountain catchment in the rain-snow transition zone. *Earth Syst. Sci. Data* 6, 165–173. <http://dx.doi.org/10.5194/essd-6-165-2014>.
- Krajewski, W.F., Lakshmi, V., Georgakakos, K.P., Jain, S.C., 1991. A Monte Carlo study of rainfall sampling effect on a distributed catchment model. *Water Resour. Res.* 27 (1), 119–128. <http://dx.doi.org/10.1029/90WR01977>.
- Kumar, M., Marks, D., Dozier, J., Reba, M., Winstral, A., 2013. Evaluation of distributed hydrologic impacts of temperature-index and energy-based snow models. *Adv. Water Resour.* 56, 77–89. <http://dx.doi.org/10.1016/j.advwatres.2013.03.006>.

- LaMontagne, A., 2009. Characterization and quantification of ground heat flux for late season shallow snow, Boise State University, Boise, ID, 69pp. <<http://scholarworks.boisestate.edu/td/48/>>.
- Link, T.E., Marks, D., 1999. Point simulation of seasonal snow cover dynamics beneath boreal forest canopies. *J. Geophys. Res.-Atmos.* 104 (D22), 27841–27857. <http://dx.doi.org/10.1029/1998JD200121>.
- Liston, G.E., 1995. Local advection of momentum, heat, and moisture during the melt of patchy snow covers. *J. Appl. Meteorol.* 34 (7), 1705–1715. <http://dx.doi.org/10.1175/1520-0450-34.7.1705>.
- Liston, G.E., Elder, K., 2006. A distributed snow-evolution modeling system (SnowModel). *J. Hydrometeorol.* 7 (6), 1259–1276. <http://dx.doi.org/10.1175/jhm548.1>.
- Liu, F., Hunsaker, C., Bales, R., 2013. Controls of streamflow generation in small catchments across the snow-rain transition in the Southern Sierra Nevada, California. *Hydrol. Process.* 27 (14), 1959–1972. <http://dx.doi.org/10.1002/hyp.9304>.
- Luce, C.H., Tarboton, D.G., Cooley, R.R., 1998. The influence of the spatial distribution of snow on basin-averaged snowmelt. *Hydrol. Process.* 12 (10–11), 1671–1683. [http://dx.doi.org/10.1002/\(sici\)1099-1085\(199808/09\)12:10<1671::aid-hyp688>3.0.co;2-n](http://dx.doi.org/10.1002/(sici)1099-1085(199808/09)12:10<1671::aid-hyp688>3.0.co;2-n).
- MacDonald, M., Pomeroy, J., Pietroniro, A., 2009. Parameterizing redistribution and sublimation of blowing snow for hydrological models: tests in a mountainous subarctic catchment. *Hydrol. Process.* 23 (18), 2570–2583.
- Marks, D., Dozier, J., 1979. Clear-sky longwave radiation model for remote alpine areas. *Archiv Fur Meteorologie Geophysik Und Bioklimatologie Serie B-Klimatologie Umweltmeteorologie Strahlungsforschung* 27 (2–3), 159–187, ISSN: 0376–1622.
- Marks, D., Dozier, J., 1992. Climate and energy exchange at the snow surface in the alpine region of the sierra-nevada. 2. Snow cover energy-balance. *Water Resour. Res.* 28 (11), 3043–3054. <http://dx.doi.org/10.1029/92wr01483>.
- Marks, D., Winstral, A., 2001. Comparison of snow deposition, the snow cover energy balance, and snowmelt at two sites in a semiarid mountain basin. *J. Hydrometeorol.* 2 (3), 213–227. [http://dx.doi.org/10.1175/1525-7541\(2001\)002<0213:cosdts>2.0.co;2](http://dx.doi.org/10.1175/1525-7541(2001)002<0213:cosdts>2.0.co;2).
- Marks, D., Kimball, J., Tingey, D., Link, T., 1998. The sensitivity of snowmelt processes to climate conditions and forest cover during rain-on-snow: a case study of the 1996 Pacific Northwest flood. *Hydrological Processes* 12(10–11), 1569–1587. <Go to ISI>://000075740100006.
- Marks, D., Domingo, J., Susong, D., Link, T., Garen, D., 1999. A spatially distributed energy balance snowmelt model for application in mountain basins. *Hydrol. Process.* 13 (12–13), 1935–1959. [http://dx.doi.org/10.1002/\(SICI\)1099-1085\(199909\)13:12/13<1935::AID-HYP868>3.0.CO;2-C](http://dx.doi.org/10.1002/(SICI)1099-1085(199909)13:12/13<1935::AID-HYP868>3.0.CO;2-C).
- Marks, D., Link, T., Winstral, A., Garen, D., 2001. Simulating snowmelt processes during rain-on-snow over a semi-arid mountain basin. In: Hutter, K. (Ed.), *Annals of Glaciology*, vol. 32, 2001. Ann. Glaciol. Int. Glaciol. Soc., Cambridge, pp. 195–202. <Go to ISI>://000171277900033.
- Marks, D., Winstral, A., Seyfried, M., 2002. Simulation of terrain and forest shelter effects on patterns of snow deposition, snowmelt and runoff over a semi-arid mountain catchment, pp. 3605–3626 doi: [10.1002/hyp.1237](http://dx.doi.org/10.1002/hyp.1237).
- Marks, D., Winstral, A., Reba, M., Pomeroy, J., Kumar, M., 2013. An evaluation of methods for determining during-storm precipitation phase and the rain/snow transition elevation at the surface in a mountain basin. *Adv. Water Resour.* 55, 98–110. <http://dx.doi.org/10.1016/j.advwatres.2012.11.012>.
- Mazurkiewicz, A.B., Callery, D.G., McDonnell, J.J., 2008. Assessing the controls of the snow energy balance and water available for runoff in a rain-on-snow environment. *J. Hydrol.* 354 (1–4), 1–14. <http://dx.doi.org/10.1016/j.jhydrol.2007.12.027>.
- McNamara, J.P., Chandler, D., Seyfried, M., Achet, S., 2005. Soil moisture states, lateral flow, and streamflow generation in a semi-arid, snowmelt-driven catchment. *Hydrol. Process.* 19 (20), 4023–4038. <http://dx.doi.org/10.1002/hyp.5869>.
- Menard, C., Essery, R., Pomeroy, J., Marsh, P., Clark, D., 2014. A shrub bending model to calculate the albedo of shrub-tundra. *Hydrol. Process.* 28 (2), 341–351. <http://dx.doi.org/10.1002/hyp.9582>.
- Molotch, N.P. et al., 2009. Ecohydrological controls on snowmelt partitioning in mixed-conifer sub-alpine forests. *Ecohydrology* 2 (2), 129–142. <http://dx.doi.org/10.1002/eco.48>.
- Moore, I.D., Grayson, R.B., Ladson, A.R., 1991. Digital terrain modeling – a review of hydrological, geomorphological, and biological applications. *Hydrol. Process.* 5 (1), 3–30. <http://dx.doi.org/10.1002/hyp.3360050103>.
- Nolin, C.W., Daly, C., 2006. Mapping “at risk” snow in the Pacific Northwest. *J. Hydrometeorol.* 7 (5), 1164–1171. <http://dx.doi.org/10.1175/jhm543.1>.
- Patterson, P.A., Neiman, K.E., Tonn, J.R., 1985. Field guide to forest plants of northern Idaho. General Technical Report INT-180. Ogden, UT: U.S. Department of Agriculture, Forest Service, Intermountain Research Station, 246p.
- Pellicciotti, F. et al., 2005. An enhanced temperature-index glacier melt model including the shortwave radiation balance: development and testing for Haut Glacier d’Arolla, Switzerland. *J. Glaciol.* 51 (175), 573–587. <http://dx.doi.org/10.3189/172756505781829124>.
- Pomeroy, J.W. et al., 1998. An evaluation of snow accumulation and ablation processes for land surface modelling. *Hydrol. Process.* 12 (15), 2339–2367. [http://dx.doi.org/10.1002/\(sici\)1099-1085\(199812\)12:15<2339::aid-hyp800>3.0.co;2-l](http://dx.doi.org/10.1002/(sici)1099-1085(199812)12:15<2339::aid-hyp800>3.0.co;2-l).
- Pomeroy, J.W., Gray, D.M., Hedstrom, N.R., Janowicz, J.R., 2002. Prediction of seasonal snow accumulation in cold climate forests. *Hydrol. Process.* 16 (18), 3543–3558. <http://dx.doi.org/10.1002/hyp.1228>.
- Pomeroy, J.W., Toth, B., Granger, R.J., Hedstrom, N.R., Essery, R.L.H., 2003. Variation in surface energetics during snowmelt in a subarctic mountain catchment. *J. Hydrometeorol.* 4 (4), 702–719. [http://dx.doi.org/10.1175/1525-7541\(2003\)004<0702:viseds>2.0.co;2](http://dx.doi.org/10.1175/1525-7541(2003)004<0702:viseds>2.0.co;2).
- Pomeroy, J., Essery, R., Toth, B., 2004. Implications of spatial distributions of snow mass and melt rate for snow-cover depletion: observations in a subarctic mountain catchment. *Ann. Glaciol.* 38 (1), 195–201. <http://dx.doi.org/10.3189/172756404781814744>.
- Pomeroy, J., Bewley, D., Essery, R., Hedstrom, N., Link, T., Granger, R., Sicart, J., Ellis, C., Janowicz, J., 2006. Shrub tundra snowmelt. *Hydrol. Process.* 20 (4), 923–941. <http://dx.doi.org/10.1002/hyp.6124>.
- Price, A.G., Dunne, T., 1976. Energy-balance computations of snowmelt in a subarctic area. *Water Resour. Res.* 12 (4), 686–694. <http://dx.doi.org/10.1029/WR012i004p00686>.
- Reba, M.L. et al., 2011a. A long-term data set for hydrologic modeling in a snow-dominated mountain catchment. *Water Resour. Res.* 47 (7). <http://dx.doi.org/10.1029/2010wr010030>.
- Reba, M.L., Marks, D., Winstral, A., Link, T.E., Kumar, M., 2011b. Sensitivity of the snowcover energetics in a mountain basin to variations in climate. *Hydrol. Process.* 25 (21), 3312–3321. <http://dx.doi.org/10.1002/hyp.8155>.
- Reba, M., Marks, D., Link, T., Pomeroy, J., Winstral, A., 2014. Sensitivity of model parameterizations for simulating latent heat flux over snow. *Hydrol. Process.* 28, 868–881. <http://dx.doi.org/10.1002/hyp.9619>.
- Rott, H., et al., 2009. ESA SP-1313/3 candidate earth explorer core missions report for assessment: CoReH2O—Cold regions hydrology high resolution observatory. In: Office, E.C.P. (Ed.), p. 114.
- Rott, H. et al., 2010. Cold regions hydrology high-resolution observatory for snow and cold land processes. *Proc. IEEE*, 98(5), 752–765. <http://ieeexplore.ieee.org/xpls/abs_all.jsp?arnumber=5420000&tag=1>.
- Scanlon, B.R. et al., 2006. Global synthesis of groundwater recharge in semiarid and arid regions. *Hydrol. Process.* 20 (15), 3335–3370. <http://dx.doi.org/10.1002/hyp.6335>.
- Schmidt, S.K., Lipson, D.A., 2004. Microbial growth under the snow: implications for nutrient and allelochemical availability in temperate soils. *Plant Soil* 259 (1–2), 1–7. <http://dx.doi.org/10.1023/B:PLSO.000020933.32473.7e>.
- Sensoy, A., Sorman, A.A., Tekeli, A.E., Sorman, A.U., Garen, D.C., 2006. Point-scale energy and mass balance snowpack simulations in the upper Karasu basin, Turkey. *Hydrol. Process.* 20 (4), 899–922. <http://dx.doi.org/10.1002/hyp.6120>.
- Seyfried, M.S., Grant, L.E., Marks, D., Winstral, A., McNamara, J., 2009. Simulated soil water storage effects on streamflow generation in a mountainous snowmelt environment, Idaho, USA. *Hydrol. Process.* 23 (6), 858–873. <http://dx.doi.org/10.1002/hyp.7211>.
- Seyfried, M., Chandler, D., Marks, D., 2011. Long-term soil water trends across a 1000-m elevation gradient. *Vadose Zone J.* 10 (4), 1276–1286. <http://dx.doi.org/10.2136/vzj2011.0014>.
- Shallcross, A.T., 2012. LiDAR Investigations of snow distribution in mountainous terrain, Boise State University, Boise, ID, 62p. <<http://scholarworks.boisestate.edu/td/349/>>.
- Singh, P., Spitzbart, G., Hubl, H., Weinmeister, H.W., 1997. Hydrological response of snowpack under rain-on-snow events: a field study. *J. Hydrol.* 202 (1–4), 1–20. [http://dx.doi.org/10.1016/S0022-1694\(97\)00004-8](http://dx.doi.org/10.1016/S0022-1694(97)00004-8).
- Surfleet, C.G., Tullis, D., 2013. Variability in effect of climate change on rain-on-snow peak flow events in a temperate climate. *J. Hydrol.* 479, 24–34. <http://dx.doi.org/10.1016/j.jhydrol.2012.11.021>.
- Susong, D., Marks, D., Garen, D., 1999. Methods for developing time-series climate surfaces to drive topographically distributed energy- and water-balance models. *Hydrol. Process.* 13 (12–13), 2003–2021. [http://dx.doi.org/10.1002/\(SICI\)1099-1085\(199909\)13:12/13<2003::AID-HYP884>3.0.CO;2-K](http://dx.doi.org/10.1002/(SICI)1099-1085(199909)13:12/13<2003::AID-HYP884>3.0.CO;2-K).
- Walter, M.T. et al., 2005. Process-based snowmelt modeling: does it require more input data than temperature-index modeling? *J. Hydrol.* 300 (1–4), 65–75. <http://dx.doi.org/10.1016/j.jhydrol.2004.05.002>.
- Weill, S., Altissimo, M., Cassiani, G., Deiana, R., Marani, M., Putti, M., 2013. Saturated area dynamics and streamflow generation from coupled surface-subsurface simulations and field observations. *Adv. Water Resour.* 59, 196–208. <http://dx.doi.org/10.1016/j.advwatres.2013.06.007>.
- Wigmosta, M.S., Vail, L.W., Lettenmaier, D.P., 1994. A distributed hydrology-vegetation model for complex terrain. *Water Resour. Res.* 30 (6), 1665–1679. <http://dx.doi.org/10.1029/94wr00436>.
- Williams, C.J., McNamara, J.P., Chandler, D.G., 2009. Controls on the temporal and spatial variability of soil moisture in a mountainous landscape: the signature of snow and complex terrain. *Hydrol. Earth Syst. Sci.* 13 (7), 1325–1336. <http://dx.doi.org/10.5194/hess-13-1325-2009>.
- Winstral, A., Marks, D., 2002. Simulating wind fields and snow redistribution using terrain-based parameters to model snow accumulation and melt over a semi-arid mountain catchment, pp. 3585–3603 doi: [10.1002/hyp.1238](http://dx.doi.org/10.1002/hyp.1238).
- Winstral, A., Marks, D., Gurney, R., 2009. An efficient method for distributing wind speeds over heterogeneous terrain. *Hydrol. Process.* 23 (17), 2526–2535. <http://dx.doi.org/10.1002/hyp.7141>.
- Winstral, A., Marks, D., Gurney, R., 2013. Simulating wind-affected snow accumulations at catchment to basin scales. *Adv. Water Resour.* 55, 64–79. <http://dx.doi.org/10.1016/j.advwatres.2012.08.011>.
- Woo, M., Heron, R., Marsh, P., 1982. Basal ice in high arctic snowpacks. *Arct. Alp. Res.* 14 (3), 251–260. <http://dx.doi.org/10.2307/1551157>.